RESEARCH ARTICLE | JANUARY 03 2025

Ultrawide bandgap semiconductor h-BN for direct detection of fast neutrons

Special Collection: Ultrawide Bandgap Semiconductors

J. Li ; A. Tingsuwatit ; Z. Alemoush ; J. Y. Lin ; H. X. Jiang

APL Mater. 13, 011101 (2025)
https://doi.org/10.1063/5.0232896

Ultrawide bandgap semiconductor h-BN for direct detection of fast neutrons

Cite as: APL Mater. 13, 011101 (2025); doi: 10.1063/5.0232896
Submitted: 10 August 2024 • Accepted: 13 December 2024 •
Published Online: 3 January 2025

J. Li, A. Tingsuwatit, Z. Alemoush, J. Y. Lin, and H. X. Jiang[a]

AFFILIATIONS

Department of Electrical and Computer Engineering, Texas Tech University, Lubbock, Texas 79409, USA

Note: This paper is part of the Special Topic on Ultrawide Bandgap Semiconductors.
[a]Author to whom correspondence should be addressed: hx.jiang@ttu.edu

ABSTRACT

III-nitride wide bandgap semiconductors have contributed on the grandest scale to many technological advances in lighting, displays, and power electronics. Among III-nitrides, BN has another unique application as a solid-state neutron detector material because the isotope B-10 is among a few elements that have an unusually large interaction cross section with thermal neutrons. A record high thermal neutron detection efficiency of 60% has been achieved by B-10 enriched h-BN detectors of 100 μm in thickness in our group. However, direct detection of fast neutrons with energies above 1 MeV is highly challenging due to the extremely low interaction cross section of fast neutrons with matter. We report the successful attainment of 0.4 mm thick freestanding h-BN 4″-diameter wafers, which enabled the demonstration of h-BN fast neutron detectors capable of delivering a detection efficiency of 2.2% in response to a bare AmBe neutron source. Furthermore, it was shown that the energy information of incoming fast neutrons is retained in the neutron pulse-height spectra. A comparison of characteristics between h-BN fast and thermal neutron detectors is summarized. Neutron detectors are vital diagnostic instruments for nuclear and fusion reactor power and safety monitoring, oil field exploration, neutron imaging and therapy, as well as for plasma and material science research. With the outstanding attributes resulting from its ultrawide bandgap (UWBG), including the ability to operate at extreme conditions of high power, voltage, and temperature, the availability of h-BN UWBG semiconductor detectors with the capability of simultaneously detecting thermal and fast neutrons with high efficiencies is expected to open unprecedented applications that are not possible to attain by any other types of neutron detectors.

I. INTRODUCTION AND BACKGROUND

III-nitrides represent the most important semiconductor system next to silicon and have already contributed on the grandest scale to technological advances in lighting, displays, and power electronics.[1–9] Among members of the III-nitride family, the crystal growth and use of h-BN as an ultrawide bandgap (UWBG) semiconductor are much less developed, although h-BN is known to possess exceptional physical properties, including an UWBG of ~6 eV,[10–12] a high breakdown field of ~12 MV/cm,[13] and high in-plane thermal conductivity of ~550 W/m K.[14] Single- and few-layer h-BN have been extensively studied as an ideal template, insulating layer, and barrier material for the construction of novel 2D structures such as graphene based heterostructures,[15] as well as a host for optically stable single photon emitters.[16,17] BN has another unique application for direct conversion solid-state neutron detectors because B-10 is one of a few isotopes that has an unusually large nuclear interaction cross section with thermal neutrons (neutrons with an energy of 25 meV) of $\sigma \sim 3840$ b (=3.84 × 10^{-21} cm^2).[18,19] This unique device application, however, requires the development of thick h-BN crystals to provide high detection efficiencies because the theoretical efficiency (η_i) (or thermal neutron absorption in h-BN) relates with the detector thickness (d) by $\eta_i = 1 - e^{-d/\lambda}$, where λ denotes the thermal neutron absorption length, which is 47 μm (237 μm) for B-10 (^{10}B) enriched (natural) h-BN.[20] Progress toward the development of h-BN quasi-bulk crystals via hydride vapor phase epitaxy (HVPE) growth has been made by our group recently, and thermal neutron detectors with a record high efficiency of 60% have been achieved by ^{10}B enriched h-BN detectors of 100 μm in thickness.[20]

Detectors that are capable of sensing both thermal and fast neutrons have many important applications in critical and emerging

areas of technologies, including nuclear and fusion reactor power and safety monitoring, nuclear security, nuclear waste management, oil field exploration, neutron imaging and therapy, fundamental research in nuclear and particle, plasma and materials sciences, and life search beyond Earth.[21–25] As such, the development of highly efficient and robust neutron detectors has attracted increasing attention recently. However, the interaction cross section between fast neutrons (neutrons with energies >1 MeV) and matter is extremely low, typically on the order of ~2 b.[19,26,27] Consequently, the detection of fast neutrons is regarded as technically challenging.

Presently existing fast neutron detectors typically employ a large volume of neutron moderation material, such as a bulky high-density polyethylene (HDPE) sphere, in conjunction with a thermal neutron detector. HDPE is used to first slow down (or moderate) fast neutrons to thermal neutrons, and then a thermal neutron detector, such as a ^{3}He gas detector, is used to detect the neutron signal, e.g., Ludlum's Bonner sphere neutron meters.[28] Because the interaction cross section of thermal neutrons with certain isotopes (e.g., ^{3}He) is several orders of magnitude larger than that of fast neutrons, the detection efficiency and count rate are, in fact, increased by implementing this moderation process. Other fast neutron detectors are based on organic scintillators,[19–21,29] in which hydrogen nuclei are scattered elastically by the incident fast neutrons to produce recoiling protons, and the kinetic energy of the recoiling particles is converted into photons, which are then detected by another photoelectric detector. The disadvantages of these types of indirect conversion fast neutron detectors include being bulky and heavy, nonportable, having a fixed operation range, being inconvenient to use, often losing the information pertaining to the energy of the incoming neutrons, and being incapable of operating in harsh conditions such as high temperatures. The feasibility of organic semiconducting single crystals for direct detection of fast neutrons has been investigated recently.[30]

We report here the attainment of the first h-BN UWBG semiconductor detector for direct detection of fast neutrons with a practical detection efficiency via the successful realization of quasi-bulk wafers with thicknesses >350 μm and multi-stacked h-BN detectors. Direct detection means that neutron interaction as well as the generation of free charge carriers and electrical signals all occur in h-BN itself, and no conversion material nor external photoelectric detector is needed. Along with its superior intrinsic physical properties resulting from UWBG, including the ability to operate at extreme conditions of high power, voltage, and temperature, h-BN direct conversion neutron detectors with practical detection efficiencies offer new functionalities that were previously impossible with other types of neutron detectors.

II. METHODS

Due to the small elastic scattering cross section (~2 b), a very thick layer of h-BN material is needed. However, presently more widely accessible h-BN bulk crystals produced by high pressure and high temperature (HPHT) and metal flux solution methods[31–37] are impractical for device fabrication as their crystallite sizes are typically smaller than a millimeter. The ability to produce large size quasi-bulk wafers (or thick epitaxial films) is needed. We have developed and produced quasi-bulk h-BN wafers using the HVPE growth technique,[20,38–40] which has a demonstrated capability to grow high quality III-nitride wide bandgap semiconductors with high growth rates. Natural boron trichloride (BCl_3) and NH_3 were used as precursors, and H_2 was used as a carrier gas.[20,38–40] The growth was conducted on 4″-diameter c-plane sapphire substrates. In contrast to the metal organic chemical vapor deposition (MOCVD) growth technique, the precursors used in HVPE growth contain no carbon impurities, and the technique also provides a growth rate that is at least an order of magnitude faster than that of MOCVD. As illustrated in Fig. 1(a), due to h-BN's layered structure, a thick h-BN wafer self-separates from the sapphire substrate after growth during the process of cooling down, from which a freestanding h-BN wafer was obtained. The as-grown h-BN freestanding quasi-bulk wafer has a thickness of ~400 μm as probed by profilometry measurement, and Fig. 1(b) shows a portion of the freestanding h-BN wafer. The x-ray diffraction (XRD) pattern obtained in a 2θ-ω scan in a large angle range is shown in Fig. 1(c). Diffraction peaks from h-BN (002) and (004) planes were clearly observable, revealing that the as-grown 400 μm thick h-BN wafer possesses a layered crystalline structure and a decent long-range order in the c-axis. The h-BN (002) peak appears at an angle of 2θ = 26.56°, corresponding to an interlayer spacing that is slightly larger than 3.33 Å, compared to 2θ = 26.72° for 100 μm thick h-BN wafers.[20] Furthermore, compared to 100 μm thick h-BN wafers,[20] the diffraction peak from h-BN (006) planes is absent in the 400 μm thick wafer. The results indicate that the stacking sequence in the c-direction deteriorates with increasing wafer thickness, and there is a lot of room for further improvement.

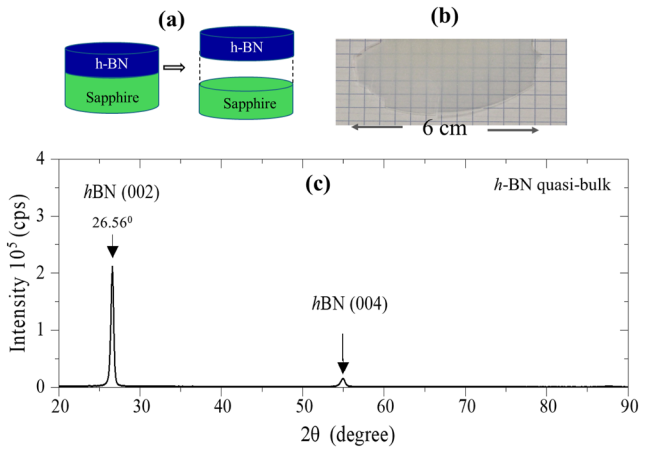

FIG. 1. (a) Schematic illustration of h-BN freestanding wafer formation. (b) Photo of a portion of an as-grown 4″-diameter h-BN quasi-bulk wafer of about 400 μm in thickness. (c) XRD pattern obtained in a 2θ-ω scan in a large angle range.

The 400 μm thick freestanding wafer was subjected to mechanical polish to thin down to about 350 μm in thickness to improve the surface smoothness and then cut into strips of 1.3 mm in width and 7.5 mm in length via laser dicing. By stacking 4 such layers together, a total thickness of 1.4 mm was achieved. Figures 2(a) and 2(b) are schematic illustrations of detectors consisting of a single stack and a four-layer vertical stacked h-BN detector. Figure 2(c) shows the optical image of a finished four-layer, vertically stacked h-BN fast neutron detector. A highly resistive adhesive material (polyimide)

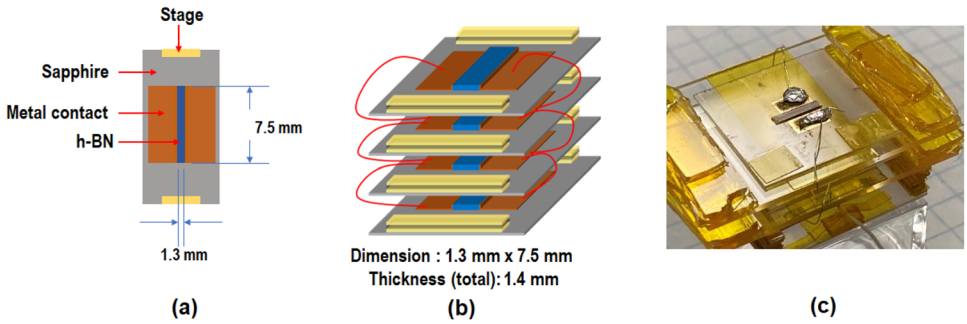

FIG. 2. Schematic diagrams of (a) a single layer h-BN detector, (b) a four-layer stacked h-BN fast neutron detector, and (c) optical image of a completed four-layer stacked h-BN detector with a total thickness of 1.4 mm with a dimension of 1.3 mm in width and 7.5 mm in length.

was used to mount the detectors onto an insulating sub-mount (sapphire). Metal contacts consisting of a bi-layer of Ni (100 nm)/Au (40 nm) were deposited on the two edges of each BN strip using e-beam evaporation via a mask. Wire bonding was then performed to electrically connect the detector strips in parallel via the bonding pads of a semiconductor device package. The use of multiple vertically stacked h-BN layers is to achieve a total thickness of 1.4 mm with the aim of realizing a practical detection efficiency. The dark current–voltage characteristics of this detector revealed a room temperature resistivity of 5×10^{13} Ω cm. Such high resistivity values translate to low background counts, which is another outstanding characteristic expected from UWBG semiconductors. Bare ^{252}Cf and AmBe neutron sources (without the use of HDPE moderators) were employed as the fast neutron sources. Neutrons emitted from the ^{252}Cf and AmBe neutron sources are in the energy range of 0–9 MeV with an average neutron energy of 2.13 MeV and 0–11 MeV with an average neutron energy of 4.2 MeV, respectively.[41–44]

III. RESULTS AND DISCUSSION

A. Mean free path of fast neutrons in h-BN

To detect fast neutrons with energy larger than 1 MeV, the process of elastic scattering of fast neutrons with the detector's constituent elements is utilized. In most cases, the elastic scattering has a relatively larger cross section compared to those of fast neutron capturing and inelastic scattering processes. In an elastic scattering process, fast neutrons are scattered elastically and transfer a fraction of their energies to the constituent elements. The recoiling element will move inside the detector material and deposit its energy by generating free electrons and holes. In using BN for fast neutron detection, after elastic scattering of fast neutrons with B and N, the energy transferred from fast neutrons to the recoiling B and N will generate free charge carriers. The collection of these charge carriers signifies the detection of fast neutrons, which follows the description below,

$$E_R = \left[\frac{4A}{(1+A)^2}\right](\cos^2\theta)E_N, \tag{1}$$

where E_R denotes the recoil energy, A is the atomic number, and A = 10, 11, and 14 for B-10 (20%), B-11 (80%), and N-14 (100%) in natural BN, θ represents the recoil angle of the recoiling element and E_N the energy of incoming neutrons. Based on Eq. (1), the recoil energy (E_R) increases with a decrease in the atomic number A. Since B and N possess the lowest atomic numbers among the constituents of all inorganic semiconductors, Eq. (1) reveals an important advantage of BN as a fast neutron detection material. At a fixed neutron energy (E_N), fast neutrons can transfer more energy (E_R) to the recoiling B and N elements and generate more free charge carriers inside BN and, hence, a higher detection efficiency in comparison to other semiconductor materials.

The mean free path of fast neutrons in h-BN can be determined by measuring the transmission of fast neutrons, as we have done previously for neutrons emitted from the ^{252}Cf source.[45] Figure 3(a) shows a schematic setup for the neutron transmission measurements. The relatively fast neutron fluxes (T) passing through pyrolytic BN (p-BN) films of different thicknesses (d) are recorded using an h-BN neutron detector. Figure 3(b) compares the transmission characteristics of fast neutrons from ^{252}Cf and AmBe neutron sources by measuring the fraction of fast neutron flux passing through pyrolytic BN films of varying thicknesses. Although pyrolytic BN films do not have the ability to collect neutron-generated free charge carriers, pyrolytic BN and h-BN have similar structural properties. Therefore, the results of fast neutron transmission measured in pyrolytic BN closely represent those in h-BN semiconductors. The measured transmission (T) of fast neutrons of these two different sources can be described by the following equation:

$$T = e^{-\frac{d}{\lambda}}, \tag{2}$$

where d is the layer thickness of BN and λ is the mean free path of fast neutrons emitted from these two sources in h-BN. The measured data can be fitted very well by Eq. (2), yielding fitted mean free paths of 7.6 and 5.2 cm for neutrons emitted from ^{252}Cf (blue squares) and AmBe (red circles) neutron sources, respectively. The measured difference in λ values among these two neutron sources reflects the fact that the neutron energy spectra are different for these two sources. Since the theoretical detection efficiency (η_i), or equivalently the mean free path of fast neutrons in h-BN, increases with the detector thickness (d) following $\eta_i = 1 - e^{-d/\lambda}$, where λ = 7.6 and 5.2 cm for fast neutrons emitted from ^{252}Cf and AmBe neutron sources, respectively, Eq. (2) implies that detectors with a thickness d > 7.6 cm (or 5.2 cm) are needed to achieve h-BN fast neutron detectors with an intrinsic detection efficiency exceeding 63% (=1 − e^{-1}) for fast neutrons with a comparable average energy as those emitted from ^{252}Cf (or AmBe) sources. For the four-layer stacked h-BN detector with a total thickness of 1.4 mm investigated here, we,

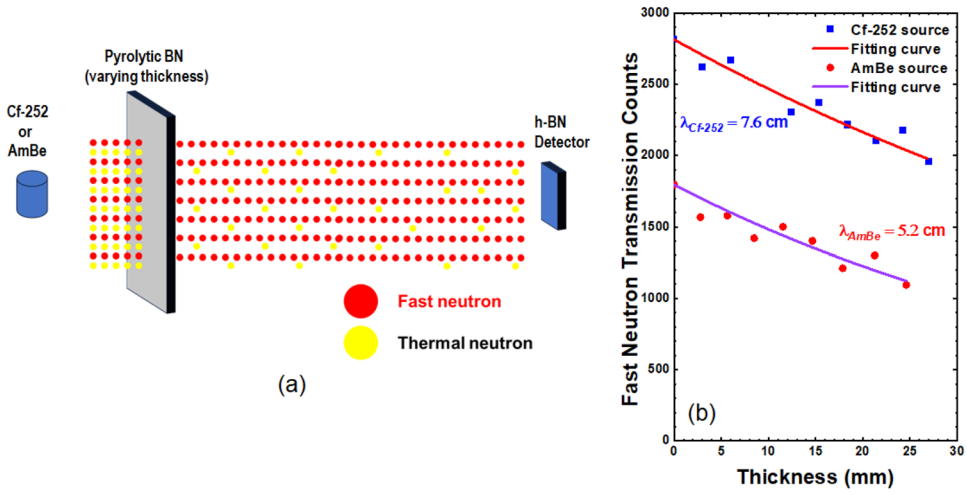

FIG. 3. (a) Schematic of the experimental setup for the neutron transmission measurements. Pyrolytic BN films were used in-lieu-of BN, and the relative neutron flux passing through pyrolytic BN films of varying thicknesses (d) was recorded using a BN semiconductor neutron detector. (b) Measured fast neutron transmission (T) as a function of BN layer thickness (d) for two neutron sources of ^{252}Cf (blue dots) and (b) AmBe (red dots circles). The solid curves are the least square fit of data with Eq. (2).

therefore, expect a maximum detection efficiency of 1.8% and 2.7% for fast neutrons emitted from ^{252}Cf and AmBe neutron sources, respectively.

B. Fast neutron detection efficiency of h-BN

To determine the detection efficiency, the detector was operated in such a way as to perform particle counting and pulse height spectrum analysis, as we have done for h-BN thermal neutron detectors.[20,45–49] Detection electronics were commercially obtained from Cremat Inc., which includes a charge sensitive preamplifier and a Gaussian-shaping amplifier. Briefly, a sharp current pulse is produced from the detector immediately after the charge carrier generation by the recoiling nucleus and subsequent collection by electrodes, which is fed into the preamplifier. This current pulse is then integrated and amplified in the charge sensitive preamplifier (model CR-110), chosen for its maximum amplification (gain: 1.4 V/pC) of the signal with minimum noise induction, to produce a voltage pulse. This pulse is further amplified and shaped using a shaping amplifier (model CR-200) to generate a Gaussian pulse, which is then fed into a multichannel analyzer (MCA) (Amptek 8000D) to sort the pulses into different energy bins based on their height and produce a histogram of incoming neutron pulse heights, known as the pulse height spectrum (PHS).[50,51] Since the height (or amplitude) of each pulse is proportional to the energy deposited inside the detector, a PHS also contains information pertaining to the distribution of the energy deposited inside the detector, or values of recoil energies (E_R) for the case of the h-BN fast neutron detector investigated here.

Because the h-BN detector is highly sensitive to thermal neutrons,[20,46–51] thermal neutrons from bare ^{252}Cf and AmBe sources (without the use of HDPE moderators) must be filtered out in order to determine the detection efficiency of h-BN for fast neutrons only. Knowing the fact that the absorption length of thermal neutrons in natural BN is 237 μm,[20,45–51] we used a pyrolytic BN film of 2.1 mm in thickness to completely block thermal neutrons from these two sources. The h-BN detector was placed 10 cm from the bare neutron sources. The measured pulsed height spectra (PHS) in response to the bare ^{252}Cf (red curve) and AmBe (blue curve) sources, as well as in the absence of any source (black curve), are shown in Fig. 4, all measured at a bias voltage of V_B = 500 V. It is worth pointing out that the sensitivity of h-BN detectors to gamma photons from the 662 keV ^{137}Cs source is at the background level because BN is composed of low atomic number elements B and N. By setting the lower-level discrimination (LLD) in the detection electronics above the response of the detector to 662 keV ^{137}Cs gamma photons, any response to gamma photons was successfully filtered out.[20,47] For the AmBe source, the neutron emission rate was 6.46 $\times$ 10^5 n/s, providing a neutron flux of 514 n/s cm^2 at 10 cm from the source. The neutron flux acquired by the h-BN detector was 11.1 n/s cm^2. This provides a measured detection efficiency of 2.2% and a charge collection efficiency of 81% by using the calculated theoretical efficiency value of 2.7% based on the measured value of the mean free path of 5.2 cm [Fig. 3(b)] for fast neutrons from the AmBe source in h-BN. For the ^{252}Cf source, the neutron emission rate was 5.60 $\times$ 10^5 n/s at the time of measurements, providing a neutron flux of 446 n/s cm^2 at 10 cm from the source. The neutron flux acquired by the h-BN detector was 2.29 n/s cm^2. This provides a measured detection efficiency of 0.51%. The measured detection efficiency of 0.5% for the ^{252}Cf source here is consistent with a value of ~0.1% measured previously for a 90 μm thick h-BN detector.[45] To the best of our knowledge, this is the first demonstration of a semiconductor detector that can detect fast neutrons directly with a measured efficiency of more than 2%. The observed fast neutron detection efficiency difference in response to these two sources reflects the difference in the neutron energy spectra since all other experimental conditions are identical.

The fast neutron PHS revealed several important characteristics: (1) The PHS covers up to 3 MeV of recoil energy instead of ~10 MeV of the fast neutron spectral range of both neutron sources. This can be explained by the relationship between the recoil energy (E_R) and fast neutron energy (E_N) described in Eq. (1). For instance, for the elastic scattering process between a neutron and the B-10 isotope, the maximum E_R relative to E_N is determined by the factor of $4A/(1 + A)^2 = (4 \times 10)/(1 + 10)^2 = 0.33$. Therefore, the energy scale for E_R is reduced to 1/3 relative to the energy scale of E_N. (2) For

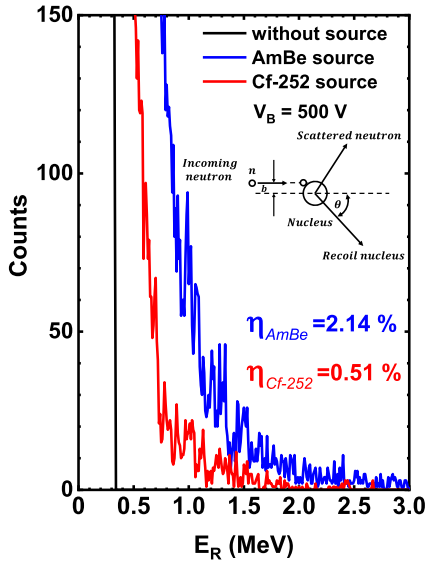

FIG. 4. Pulsed height spectra (PHS) acquired by the 1.4 mm thick h-BN fast neutron detector in response to fast neutrons from bare ^{252}Cf source (red curve) and AmBe source (blue curves) without the use of an HDPE moderator and in the absence of any source (black curve), all measured at a bias voltage V_B = 500 V and at 10 cm from the sources. A p-BN of 2.1 mm in thickness is used to block any thermal neutrons from these two neutron sources. The inset illustrates the relationship between the impact parameter *b* and recoil angle θ of recoiling elements in the elastic scattering process.

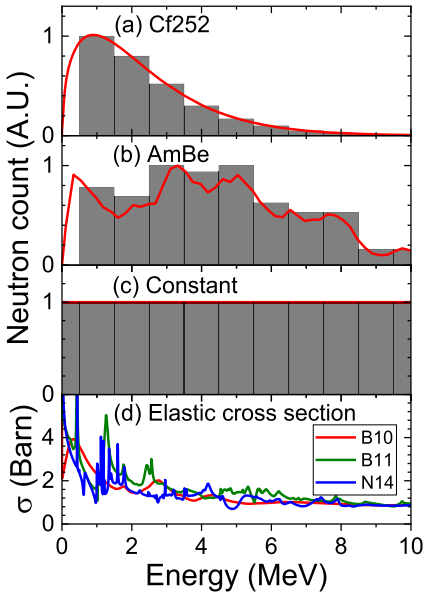

FIG. 5. Energy spectra of neutron sources used in the Monte Carlo N-Particle Transport Code (MCNP) 6.3 simulation: (a) Cf-252, (b) AmBe, and (c) a hypothetical neutron source with a constant emission rate. The emission spectra of the neutron sources have been divided into 10 sections for simulation. (d) Elastic scattering cross sections of fast neutrons with isotopes of B-10, B-11, and N-14 below 10 MeV.

both neutron sources, detected counts decrease with an increase of E_R. This is due to the recoil angle dependence of the recoil energy described by Eq. (1), to be discussed in more detail with simulation results. (3) The same h-BN detector delivers higher detection efficiency in response to fast neutrons from the AmBe source than to neutrons from the ^{252}Cf source because the average neutron energy emitted from the AmBe source is higher than that from the ^{252}Cf source. Higher energy neutrons can transfer more energy to recoiling B and N during elastic scattering, generating more electrons and holes and, hence, more events of collected charge carriers above the noise level or LLD. The detection efficiency measurement results, therefore, indicate that h-BN is more suitable for detecting neutrons with higher energies.

C. MCNP simulation results

To further understand the characteristics of the measured PHS discussed above, we carried out Monte Carlo N-Particle Transport Code (MCNP) 6.3 to simulate the PHS of natural h-BN detectors in responses to fast neutrons from both ^{252}Cf and AmBe neutron sources. To do this, we first reproduced the neutron energy spectra of these sources, as shown in Fig. 5(a) for ^{252}Cf and Fig. 5(b) for AmBe. To investigate the effects due to variations in the neutron energy spectra, we also introduced a hypothetical neutron source with a constant emission rate from 0 to 10 MeV, as shown in Fig. 5(c). Figure 5(d) plots the energy dependence of the elastic scattering cross section of fast neutrons with B-10, B-11, and N-14. In the simulation setup, an incident neutron beam with a fixed energy is introduced to interact with an h-BN cube (2 × 2 × 2 mm^3). The energy spectra of the neutron sources are divided into 10 sections from 1 to 10 MeV, each segment covering a spectral width of 1 MeV as illustrated in Fig. 5. For each neutron energy segment, we collected the total counts of scattered neutrons at different scattering angles ranging from 0 to 180° with a step of every 15°. Based on the principle of energy conservation, the recoil energy (E_R) of B-10, B-11, and N-14 can be determined from the energies of fast neutrons before (E_N) and after (E'_N) elastic scattering, $E_R = E_N - E'_N$.

For each section of incident neutron energy from 1 to 10 MeV, the total counts of scattered neutrons as functions of neutron energy at each collected angle can be obtained from simulation. The normalized simulated PHS, or the total counts vs recoil energy (E_R) in response to ^{252}Cf (green curve), ^{241}Am^{9}Be (blue curve), and the hypothetical neutron source of Fig. 5(c) with a constant emission rate (red curve) between 0 and 10 MeV, have been obtained and are plotted in Fig. 6. The simulation results incorporate the emission spectra of neutron sources as well as the contribution from each energy segment of fast neutrons, as described in Fig. 5. Comparing the PHS in the presence of ^{252}Cf and AmBe sources with the constant rate source provides us with insights pertaining to the effects resulting from the difference in the neutron energy spectra. It is worth mentioning that the steps in the simulated PHS of Fig. 6 are an artifact of dividing the neutron spectra of ^{252}Cf and AmBe sources into 10 sections with 1 MeV in each section. The use of only 10 segments is to limit the total simulation time. These steps are expected to disappear if the total number of sections is increased.

Several important conclusions can be drawn by comparing the simulated and measured PHS. First, measured and simulated

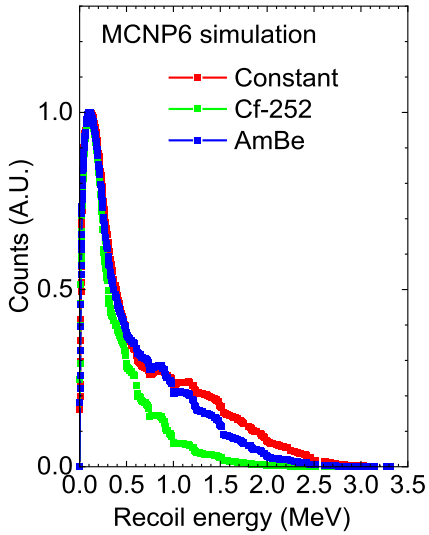

FIG. 6. Normalized simulated pulse height spectra (PHS) of h-BN fast neutron detectors in response to different neutron sources of ^{252}Cf (green curves), AmBe (blue curves), and constant emission rates between 1 and 10 MeV. The emission spectra of the neutron sources have been divided into 10 sections for simulation.

PHS are similar, providing us with confidence in interpreting these results. Second, the simulated counts decrease with the recoil energy, E_R, following the same trend as the measured PHS shown in Fig. 4, which is true for all three sources simulated, including the hypothetical neutron source with a constant emission rate. Therefore, the observed count rate decreasing with E_R is not caused by the difference in the emission energy spectra of neutron sources because this behavior was also observed for the source with a constant emission rate. Finally, the trend of the count rate decreasing with E_R is not caused by the energy dependence of the elastic scattering cross section because its variation in the range from 1 to 10 MeV is rather weak, as shown in Fig. 5(d).

The count rate decreasing with E_R exhibited by both the measured and simulated PHS can be understood by the following interpretation. As shown in the inset of Fig. 4, the recoil angle θ depends on the impact parameter (b) of the incoming fast neutrons, and θ increases with b. The count rate is proportional to 2πb and, hence, increases with θ. However, according to Eq. (1), $E_R \propto \cos^2\theta$, meaning a larger value of E_R corresponds to a smaller value of θ, whereas a smaller recoil angle θ means a lower probability of elastic scattering events (or a smaller value of b) and, hence, lower counts. The count rate is, therefore, expected to decrease with E_R. It is interesting to note that in the region of higher E_R values, the count rate decreases fastest for the ^{252}Cf source, then followed by the AmBe source, and slowest for the constant rate neutron source. This behavior can be accounted for by the variations in the emission spectra of these three neutron sources displayed in Fig. 5, which shows that the neutron emission rate of the ^{252}Cf source decreases exponentially with E_N beyond 1 MeV,[41,42] and consequently, the measured count rate decreases fastest with E_R for neutrons emitted from ^{252}Cf among the three neutron sources.

D. Characteristics comparison between h-BN fast and thermal neutron detectors

Table I shows the comparison of h-BN direct conversion thermal and fast neutron detectors. While h-BN can detect both thermal and fast neutrons, the principles and mechanisms, as well as the detector parameters, are very different. These differences include (1) the operating principle of thermal neutron detection, which is based on the processes of nuclear reaction (or absorption) of a thermal neutron by B-10, charge carrier generation by the nuclear reaction products, and charge carrier collection,[19,20,45–57] whereas the detection of fast neutrons is based on the processes of energy transfer of fast neutrons to the B and N through elastic scattering, charge carrier generation by recoil B and N, and charge carrier collection. Therefore, only the B-10 isotope is involved in the thermal neutron

TABLE I. Comparison of h-BN fast and thermal neutron detectors.

Neutrons	Thermal neutrons	Fast neutrons
Neutron energy (E_N)	0.025 eV	>1 MeV
Principle	Nuclear reaction	Elastic scattering
Mechanism	${}^{10}_{5}B + {}^{1}_{0}n = {}^{7}_{3}Li^* + {}^{4}_{2}\alpha^*[94\%]$ ${}^{10}_{5}B + {}^{1}_{0}n^{7}_{3}Li + {}^{4}_{2}\alpha[6\%]$	n + X → n' + X' (X' = $^{10}B^+$, $^{11}B^+$, $^{14}N^+$)
Secondary particles	Li^*, Li, α^*, α	$^{10}B^+$, $^{11}B^+$, $^{14}N^+$
Charge generation	Li^*, Li, α^*, α → e^- + h^+	$^{10}B^+$, $^{11}B^+$, $^{14}N^+$ → e^- + h^+
E_N information	Lost	Retained
Cross section (b)	3740	~2
Absorption length (or mean free path)<	100 s μm	~6 cm
Range of secondary particles	Li^*, Li = 2 μm, α^*, α = 5 μm	X' < 2 μm (X' = $^{10}B^+$, $^{11}B^+$, $^{14}N^+$)
Energy deposited	Discreate Li^* = 0.84 MeV, α^* = 1.47 MeV Li = 1.015 MeV, α = 1.777 MeV	Continuous $E_R(\theta) = \left[\frac{4A}{(1+A)^2}\right](\cos^2\theta)E_N$
Detection efficiency	Constant	Higher for higher E_N

absorption process for thermal neutron detection. However, all constituent elements of B-10, B-11, and N-14 in h-BN are involved in the processes of elastic scattering for fast neutron detection. (2) The energies of nuclear reaction products in the thermal neutron detection processes have discrete values, such as $Li^* = 0.84$ MeV and $\alpha^* = 1.47$ MeV,[19] whereas the recoil energy (E_R) after elastic scattering with an incoming neutron of energy E_N covers a continuous spectrum with a minimum value of $E_R = 0$ and a maximum value of $E_R = [4A/(1 + A)^2]E_N$ corresponding to a recoil angle of recoiling elements of 90° and 0°, respectively. (3) It is possible to detect fast neutrons directly without the need to use an HDPE moderator with a detection efficiency of 10% or more if the total thickness of h-BN can reach ~1 cm. Replacing existing neutron detectors that incorporate HDPE conversion materials (such as the Bonner sphere detector) with solid-state direct conversion detectors will dramatically reduce the overall system size and weight. (4) Information of fast neutron energy is lost if HDPE is used since the scattering of fast neutrons with H atoms inside HDPE is a random process, whereas the energy information of incoming fast neutrons is retained using h-BN fast neutron detectors. Our results indicate that not only can we use h-BN to directly detect neutron radiation, but we may also extract information pertaining to the energy of incoming fast neutrons. For example, the highest measured E_R value directly reflects the energy of fast neutrons if the incident neutrons are monoenergetic. This feature will open novel applications for semiconductor neutron detectors. (5) The detection efficiency of h-BN fast neutron detectors depends on neutron energy (E_N) via the energy dependence of the cross section of the elastic scattering as well as the recoil energy (E_R). On average, fast neutrons with larger energies will generate more electrons and holes in h-BN, and thus, they are easier to be detected by h-BN.

IV. CONCLUSIONS AND FUTURE WORK

In summary, direct detection of fast neutrons by h-BN UWBG semiconductor detectors has been demonstrated. A detection efficiency as high as 2.2% has been achieved by a stacked detector with a total thickness of 1.4 mm in response to neutrons emitted from a bare AmBe neutron source. The measured pulsed height spectra revealed that the count rate decreases with the recoil energy of constituent isotopes (E_R). Simulated PHS using the MCNP program is consistent with the measured PHS. The results showed that for a fixed neutron energy, E_N, the probability of elastic scattering decreases with increasing the recoil energy (E_R), resulting from the fact that E_R decreases with the recoil angle (θ) following the relationship of $E_R \propto \cos^2\theta$. The availability of a new class of fast neutron detectors based on h-BN UWBG semiconductors is expected to dramatically enhance the functionalities of semiconductor neutron detectors as well as open novel applications in nuclear and fusion reactor power and safety monitoring, oil field exploration, neutron imaging and therapy, as well as for plasma and material science research. The demonstration of h-BN UWBG semiconductor neutron detectors further justifies the need for a concerted effort by the field to collectively advance the UWBG semiconductor material and device technologies. For neutron detector applications, the development of h-BN bulk crystals with large wafer sizes and centimeters in thickness with high crystalline quality is needed to enable the realization of fast neutron detectors with an efficiency exceeding 10% as well as the construction of larger area detectors to provide high detection sensitivities (high neutron flux).

ACKNOWLEDGMENTS

The information, data, or work presented herein was funded in part by the Advanced Research Projects Agency-Energy (ARPA-E), U.S. Department of Energy, under Award No. DE-AR0001552 and was monitored by Dr. Olga Spahn and Dr. Eric Carlson. The views and opinions of authors expressed herein do not necessarily state or reflect those of the United States Government or any agency thereof. Jiang and Lin are grateful to the AT & T Foundation for the support of Ed Whitacre and Linda Whitacre endowed chairs.

AUTHOR DECLARATIONS

Conflict of Interest

The authors have no conflicts to disclose.

Author Contributions

J. Li: Conceptualization (equal); Data curation (equal); Formal analysis (equal); Funding acquisition (equal); Investigation (equal); Methodology (equal); Project administration (equal); Resources (equal); Software (equal); Supervision (equal); Validation (equal); Visualization (equal). **A. Tingsuwatit**: Data curation (equal); Formal analysis (equal); Investigation (equal); Methodology (equal); Software (equal); Validation (equal); Visualization (equal). **Z. Alemoush**: Data curation (equal); Formal analysis (equal); Investigation (equal); Methodology (equal); Software (equal); Validation (equal); Visualization (equal). **J. Y. Lin**: Conceptualization (equal); Formal analysis (equal); Funding acquisition (equal); Investigation (equal); Methodology (equal); Project administration (equal); Resources (equal); Supervision (equal); Validation (equal); Visualization (equal); Writing – original draft (equal); Writing – review & editing (equal). **H. X. Jiang**: Conceptualization (equal); Formal analysis (equal); Funding acquisition (equal); Investigation (equal); Methodology (equal); Project administration (equal); Resources (equal); Supervision (equal); Validation (equal); Visualization (equal); Writing – original draft (equal); Writing – review & editing (equal).

DATA AVAILABILITY

The data that support the findings of this study are available within the article.

REFERENCES

[1] See https://www.nobelprize.org/prizes/physics/2014/press-release/ for the Nobel Prize in Physics, 2014.
[2] S. Pimputkar, J. S. Speck, S. P. DenBaars, and S. Nakamura, Nat. Photonics **3**, 180 (2009).
[3] H. Amano, N. Sawaki, I. Akasaki, and Y. Toyoda, Appl. Phys. Lett. **48**, 353 (1986).
[4] S. Nakamura, T. Mukai, and M. Senoh, Appl. Phys. Lett. **64**, 1687 (1994).
[5] T. D. Moustakas, U.S. Patent 5,686,738 (Nov. 11, 1997).

[6]H. X. Jiang and J. Y. Lin, Nat. Electron. **6**, 257 (2023).
[7]P. J. Parbrook, B. Corbett, J. Han, T. Y. Seong, and H. Amano, Laser Photonics Rev. **15**, 2000133 (2021).
[8]H. Amano, Y. Baines, E. Beam *et al.*, J. Phys. D: Appl. Phys. **51**, 163001 (2018).
[9]M. Higashiwaki, R. Kaplar, J. Pernot, and H. Zhao, Appl. Phys. Lett. **118**, 200401 (2021).
[10]T. Sugino, K. Tanioka, S. Kawasaki, and J. Shirafuji, Jpn. J. Appl. Phys., Part 2 **36**, L463 (1997).
[11]B. Arnaud, S. Lebe'gue, P. Rabiller, and M. Alouani, Phys. Rev. Lett. **96**, 026402 (2006).
[12]G. Cassabois, P. Valvin, and B. Gil, Nat. Photonics **10**, 262 (2016).
[13]Y. Hattori, T. Taniguchi, K. Watanabe, and K. Nagashio, Appl. Phys. Lett. **109**, 253111 (2016).
[14]C. Yuan, J. Li, L. Lindsay, D. Cherns, J. W. Pomeroy, S. Liu, J. H. Edgar, and M. Kuball, Commun. Phys. **2**, 43 (2019).
[15]A. K. Geim and I. V. Grigorieva, Nature **499**, 419 (2013).
[16]R. Bourrellier, S. Meuret, A. Tararan, O. Stephan, M. Kociak, L. H. G. Tizei, and A. Zobelli, Nano Lett. **16**, 4317 (2016).
[17]T. T. Tran, C. Elbadawi, D. Totonjian, C. J. Lobo, G. Grosso, H. Moon, D. R. Englund, M. J. Ford, I. Aharonovich, and M. Toth, ACS Nano **10**, 7331 (2016).
[18]O. Osberghaus, Z. Phys. **128**, 366 (1950).
[19]G. F. Knoll, *Radiation Detection and Measurement*, 4th ed. (John Wiley & Sons, Hoboken, NJ, 2010).
[20]Z. Alemoush, A. Tingsuwatit, A. Maity, J. Li, J. Y. Lin, and H. X. Jiang, J. Appl. Phys. **135**, 175704 (2024).
[21]R. C. Runkle, Nucl. Instrum. Methods Phys. Res., Sect. A **652**, 37 (2011).
[22]U. WoŹnicka, J. Fusion Energy **38**, 376 (2019).
[23]G. Ericsson, J. Fusion Energy **38**, 330 (2019).
[24]B. M. van der Ende, L. Li, D. Godin, and B. Sur, Nat. Commun. **10**, 1959 (2019).
[25]O. Searfus, P. Marleau, E. Uribe, H. Reedy, and I. Jovanovic, Phys. Rev. Appl. **20**, 064038 (2023).
[26]J. R. Dunning, G. B. Pegram, G. A. Fink, and D. P. Mitchell, Phys. Rev. **48**, 265 (1935).
[27]T. Jevremovic, *Nuclear Principles in Engineering*, 2nd ed. (Springer Science+Business Media, LLC, 2009).
[28]Ludlum Measurements, available at https://ludlums.com/images/data_sheets/Ludlum-Neutron-Meters.pdf.
[29]S. V. Budakovsky, N. Z. Galunov, N. L. Karavaeva, J. K. Kim, Y. K. Kim, O. A. Tarasenko, and E. V. Martynenko, IEEE Trans. Nucl. Sci. **54**, 2734 (2007).
[30]D. Zhao, P. Cai, W. Cheng, W. Jia, B. Zhang, M. Zhu, L. Liu, X. Ouyang, P. Sellin, W. Jie, and Y. Xu, Adv. Funct. Mater. **32**, 2108857 (2022).
[31]T. Ishii and T. Sato, J. Cryst. Growth **61**, 689 (1983).
[32]K. Watanabe, T. Taniguchi, and H. Kanda, Nat. Mater. **3**, 404 (2004).
[33]Y. Kubota, K. Watanabe, O. Tsuda, and T. Taniguchi, Science **317**, 932 (2007).
[34]Y. Hattori, T. Taniguchi, K. Watanabe, and K. Nagashio, ACS Appl. Mater. Interfaces **8**, 27877 (2016).
[35]N. D. Zhigadlo, J. Cryst. Growth **402**, 308 (2014).
[36]J. Li, J. Wang, X. Zhang, C. Elias, G. Ye, D. Evans, G. Eda, J. M. Redwing, G. Cassabois, B. Gil, P. Valvin, R. He, B. Liu, and J. H. Edgar, Chem. Mater. **32**, 5066 (2020).
[37]J. H. Edgar, T. B. Hoffman, B. Clubine, M. Currie, X. Z. Du, J. Y. Lin, and H. X. Jiang, J. Crystal Growth **403**, 110 (2014).
[38]Z. Alemoush, N. K. Hossain, A. Tingsuwatit, M. Almohammad, J. Li, J. Y. Lin, and H. X. Jiang, Appl. Phys. Lett. **122**, 012105 (2023).
[39]Z. Alemoush, A. Tingsuwatit, J. Li, J. Y. Lin, and H. X. Jiang, Crystals **13**, 1319 (2023).
[40]A. Tingsuwatit, N. K. Hossain, Z. Alemoush, M. Almohammad, J. Li, J. Y. Lin, and H. X. Jiang, Appl. Phys. Lett. **124**, 162105 (2024).
[41]F. H. Frohner, Nucl. Sci. Eng. **106**, 345 (1990).
[42]F. D. Becchetti, M. Febbraro, R. Torres-Isea, M. Ojaruega, and L. Baum, Am. J. Phys. **81**, 112 (2013).
[43]J. W. Marsh, D. J. Thomas, and M. Burke, Nucl. Instrum. Methods Phys. Res., Sect. A **366**, 340 (1995).
[44]E. A. Lorch, Int. J. Appl. Radiat. Isot. **24**, 585 (1973).
[45]A. Tingsuwatit, A. Maity, S. J. Grenadier, J. Li, J. Y. Lin, and H. X. Jiang, Appl. Phys. Lett. **120**, 232103 (2022).
[46]H. X. Jiang, J. Y. Lin, J. Li, A. Maity, and S. J. Grenadier, "Solid-state neutron detector," US patent 10,714,651 (July 14, 2020) and US patent 11,195,968 (Dec. 7, 2021).
[47]A. Maity, S. J. Grenadier, J. Li, J. Y. Lin, and H. X. Jiang, Appl. Phys. Lett. **116**, 142102 (2020).
[48]A. Maity, S. J. Grenadier, J. Li, J. Y. Lin, and H. X. Jiang, Prog. Quantum. Electron. **76**, 100302 (2021).
[49]S. J. Grenadier, A. Maity, J. Li, J. Y. Lin, and H. X. Jiang, "Chapter 12—Electrical transport properties of hexagonal boron nitride epilayers," Semicond. Semimetals **107**, 393–454 (2021).
[50]S. J. Grenadier, "Advancements in hexagonal boron nitride for thermal neutron detection applications," Ph.D. thesis, Texas Tech University, 2020.
[51]A. Maity, "Highly sensitive hexagonal boron nitride thermal neutron detectors," Ph.D. thesis, Texas Tech University, 2020.
[52]J. Li, A. Maity, S. J. Grenadier, J. Y. Lin, and H. X. Jiang, Appl. Phys. Lett. **118**, 092102 (2021).
[53]F. P. Doty, "Boron nitride solid-state neutron detector," Report No. SAND2003-8796 (Sandia National Laboratories, Livermore, CA, 2003); US patent 6,727,504 (Apr. 27, 2004).
[54]K. Osberg, N. Schemm, S. Balkir, J. I. Brand, M. S. Hallbeck, P. A. Dowben, and M. W. Hoffman, IEEE Sens. J. **6**, 1531 (2006).
[55]R. J. Nikolic, A. M. Conway, C. E. Reinhardt, R. T. Graff, T. F. Wang, N. Deo, and C. L. Cheung, Appl. Phys. Lett. **93**, 133502 (2008).
[56]R. J. Nikolic, C. Li Cheung, C. E. Reinhardt, and T. F. Wang, Proc. SPIE **6013**, 601305 (2005).
[57]A. M. Conway, T. F. Wang, N. Deo, C. L. Cheung, and R. J. Nikolic, IEEE Trans. Nucl. Sci. **56**, 2802 (2009).